Supplementary Materials for

Label-Free Optical Differentiation of Single Diffusing Amino Acids at Picomolar Concentrations

Julia K. Rasch, Anna L. Clayborn, Daniel Sole-Barber, Sushu Wan, Carlos A. Saavedra, Alex J. Fairhall, Frank Hu, Jeffrey Bartz, Yulia Podorova, Anders J. Bergsten, Z. Donte' Young, Itzel D. Ruiz Barrera, T. H. Kendrixe Mone, Nasrin Asgari, Thomas E. Markland, Randall H. Goldsmith

Contents

1 Detection Regime Details

1.1 Comparison of Old and New Detection Regime

Figure S1 visually compares the differences between the old detection regime and the new detection regime. The left column depicts the detection regime reported here and the right column depicts the detection regime reported in Needham et al[1]. Here, by tuning the system parameters differently the same molecule can produce qualitatively different locked FFPC responses.

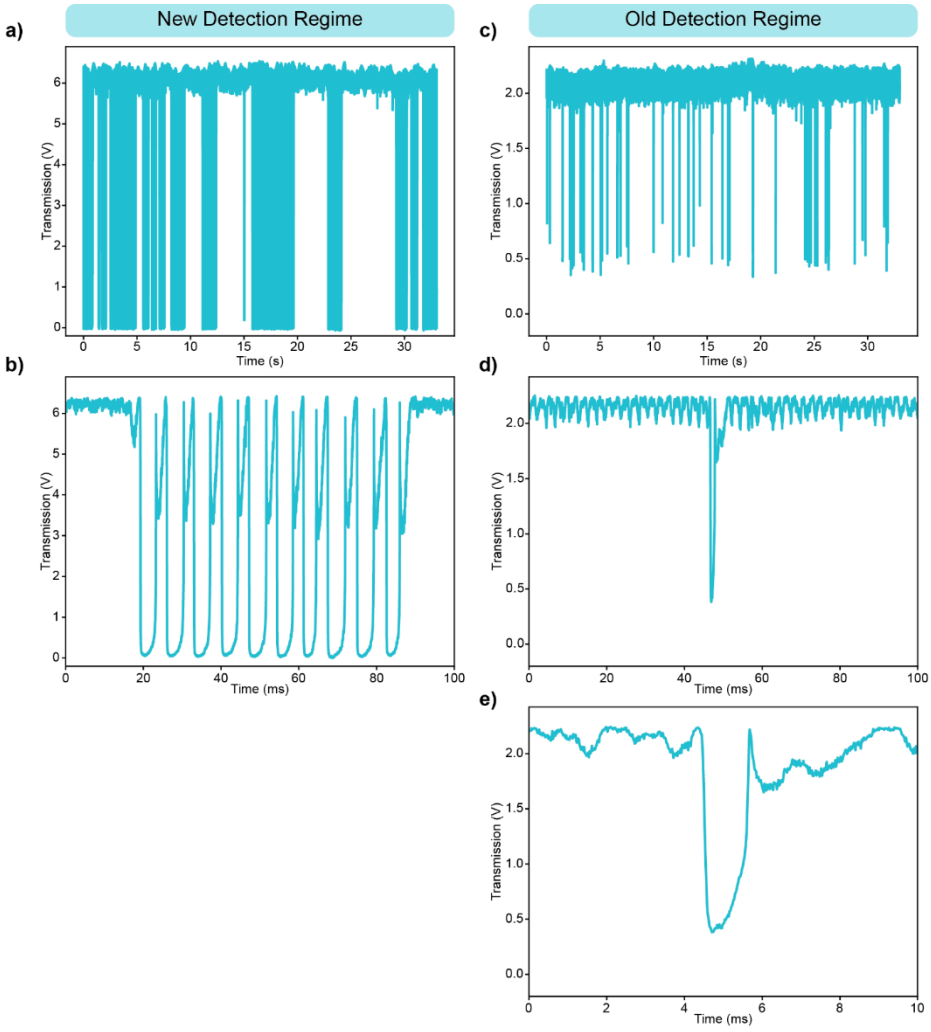

Figure S1 a-b) Transmission over time plots of signal from Myc-tag (15 pM) in the new detection regime, where a) is a 30 second trace and b) is a 100 millisecond zoom of a series of peaks. c-e) Transmission over time plots of signal from Myc-tag (16 pM) from the previously reported detection regime from Ref 1, where c) is a 30 second trace, d) is a 100 millisecond zoom of a peak, and e) is a 10 millisecond zoom of the peak in d.

1.2 Peak Saturation and Shape

As has been discussed, the burst peaks are saturating and reaching a floor. This floor is not the detector floor but a local minimum due to the sidebands applied for PDH locking. Evidence of this can be seen in Figure S2, in which the drop in transmission caused by a perturbation to the FFPC saturates to the amplitude of the sideband. This saturation behavior along with the burst effect delivers higher sensitivity, but results in a loss of information in the peak widths, precluding the hydrodynamic profiling reported in Needham et al[1].

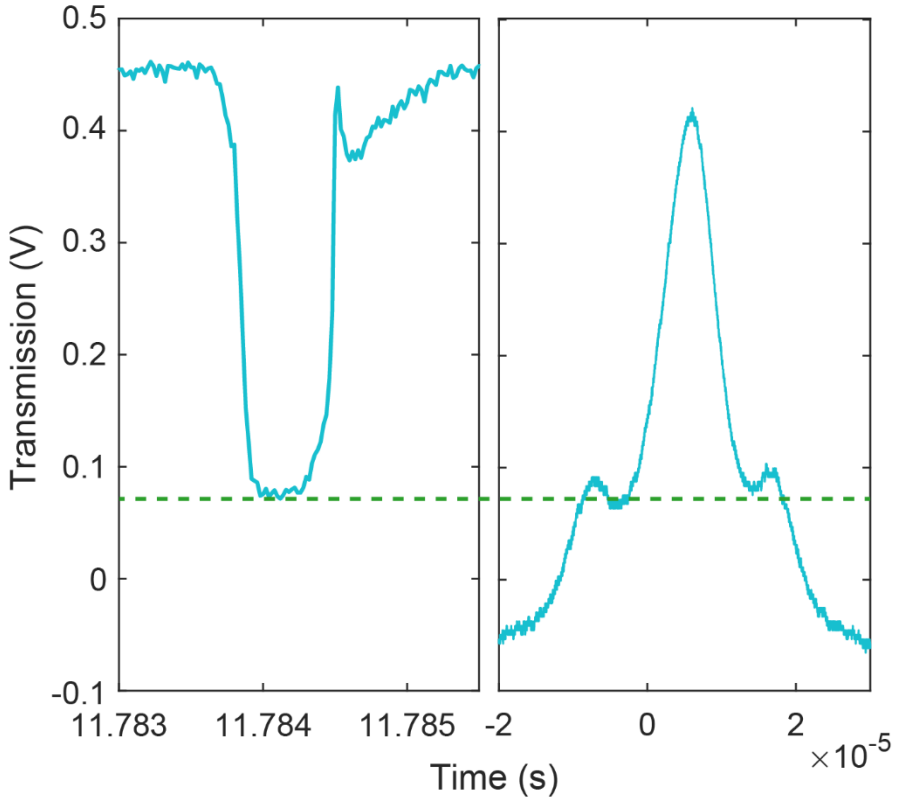

Figure S2 a) A transmission over time plot showing saturating behavior where the drop in transmission hits a floor which corresponds to the amplitude of the sidebands. b) A transmission over time plot showing the resonance with sidebands at the same amplitude as the saturating peak.

The autocorrelation plot in Figure S3 further demonstrates this behavior. This plot compares two alanine and glycine comparison experiments. In experiment 1, data was recorded for alanine and glycine using one set of system parameters, and in experiment 2, data was recorded for alanine and glycine using a different set of system parameters. Here, the data for alanine and glycine taken using the same set of system parameters is more similar than when comparing alanine in experiment 1 to alanine in experiment 2. This trend demonstrates that the peak widths are governed not by molecular motion but by small differences in locked FFPC system parameters.

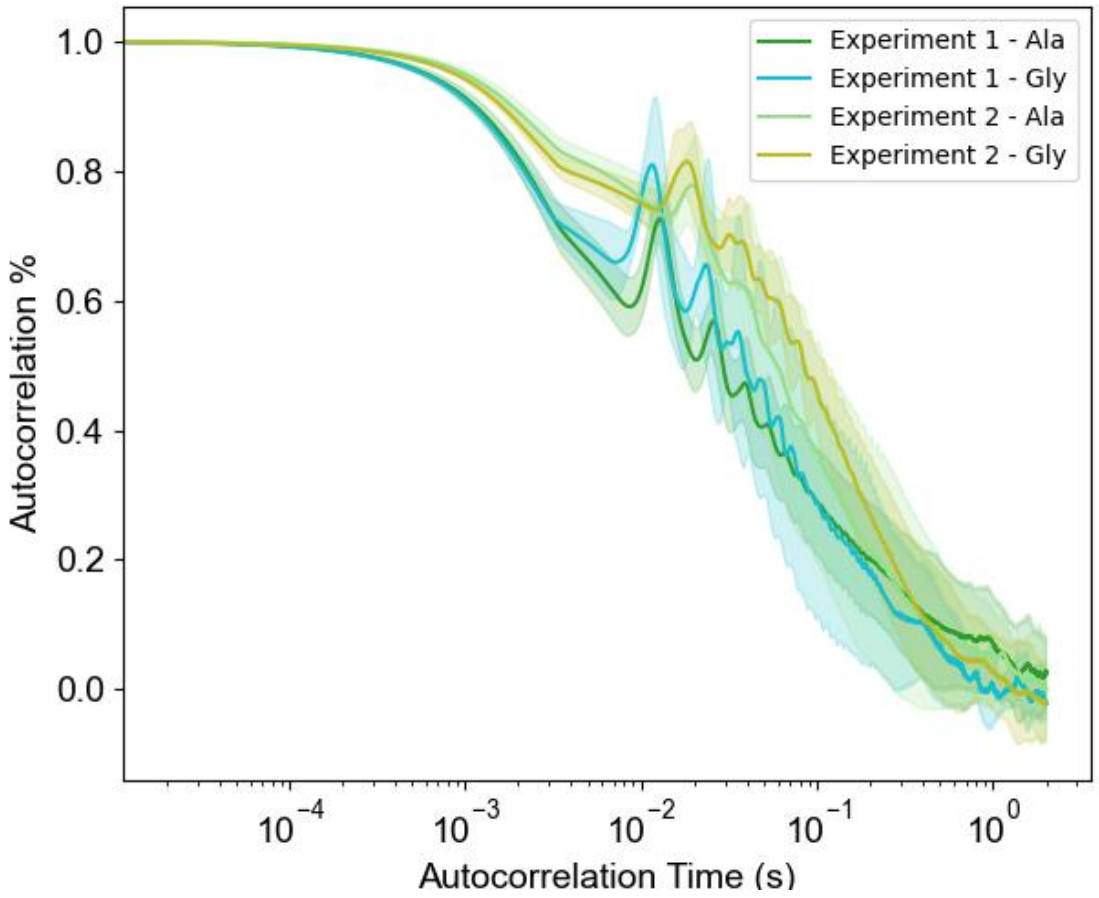

Figure S3 Autocorrelation curves depicting the dependence of peak width on input system parameters. In experiment 1, alanine and glycine data were recorded using the exact same system parameters. In experiment 2, alanine and glycine data were recorded using the exact same parameters, but the system parameters were different from experiment 1.

2 Quantitative Model and Polarizability Calculations

2.1 Quantitative Model

Simulations are performed using custom MATLAB code based on the theory developed in Saavedra et al[2]. This code functions as a series of discrete steps. First, a random walk for a molecule is generated based on its diffusion coefficient, inversely proportional to its hydrodynamic radius. The position of the molecule is tracked as it

traverses the FFPC mode, calculated geometrically using a Gaussian-envelope standing wave FFPC mode. Two methods of interaction are considered here: resonance shift, a movement of the resonant wavelength of the FFPC based on the instantaneous change to the refractive index, and a more minor effect, scattering loss, a loss of power to the environment due to scattering from the molecule. The effects of these two behaviors are calculated for the full time of the random walk. Once these calculations are complete, these dynamics are injected into the second main part of the code, where the dynamics of two key wavelengths are calculated in the presence of a static narrow band pump wavelength. One is the "cold" FFPC wavelength, affected by the locking PI feedback loop, noise estimated from previous experimental characterization,[3] and the resonance shift due to the molecule as calculated above. The second is the hot FFPC wavelength, a value based on the cold FFPC wavelength in addition to the thermal parameters of the system and scattering loss due to the molecule. The transmission through this FFPC is then calculated as an overlap integral between the pump and hot FFPC wavelengths.

2.1.1 Specific Parameters Used to Generate Data in Figure 3

To generate a burst-firing event for Tryptophan in simulations, the following parameters were set: Diffusion Coefficient – 562 μm^2/s calculated using the inverse relationship between hydrodynamic radius[4] and diffusion coefficient, molecule polarizability* - 3.11e-39 $A^2s^4kg^{-1}$, mirror diameter – 20 μm, mirror ROC – 30 μm, FFPC Length – 10 μm, input power – 28.1 μW, set Point – 0.017484, integrator gain – 0.99 nm/s, proportional gain – 0.09 pm/s, Finesse (water) – 55000, Finesse (air) – 85000, heat capacity – 4e-10 J/K, and thermal Conductance – 8.18e-5 W/K. The set point is a unitless quantity related to the position of the lock relative to the center of the resonance peak.[2]

*This value is 28 $Å^3$ (see section 2.2) multiplied by $4\pi\varepsilon_0$.

2.2 Calculation of excess polarizability for single amino acids

2.2.1 System preparation

Three aqueously solvated amino acid systems were prepared: alanine, histidine, and tryptophan. Each amino acid was prepared in its zwitterionic form using the ChimeraX[5] software to generate an initial structure. Each amino acid was then solvated with water molecules using the system modeler in OpenMM[6] with the CHARMM36 forcefield[7] and the TIP3P[8] water model. For each amino acid, solvated systems containing 256, 356, 456, and 556 water molecules with one instance of the amino acid were prepared, as well as the corresponding pure water box for a total of 16 systems. The box dimensions for each system are as follows (all boxes are cubic):

System	Box length (Å)
Water 256	19.970
Alanine + Water 256	20.098
Histidine + Water 256	20.117
Tryptophan + Water 256	20.156
Water 356	22.199
Alanine + Water 356	22.363
Histidine + Water 356	22.383
Tryptophan + Water 356	22.578
Water 456	24.257
Alanine + Water 456	24.326
Histidine + Water 456	24.385
Tryptophan + Water 456	24.395
Water 556	25.892
Alanine + Water 556	25.947
Histidine + Water 556	25.957
Tryptophan + Water 556	26.055

2.2.2 System simulation

Each system was then simulated using OpenMM with the CHARMM36 forcefield under NVT conditions with periodic boundary conditions using a Langevin Integrator at a temperature of 300K, with a friction coefficient of 1 ps^{-1}, and a time step of 0.5 fs. Following a 5 ps equilibration period, each simulation was carried out for a total of 1 ns,

with configurations saved every 50 ps. This resulted in a total of 20000 configurations for each trajectory, which were used for analysis.

System	Number of configurations
Water 256	100
Alanine + Water 256	100
Histidine + Water 256	100
Tryptophan + Water 256	98
Water 356	100
Alanine + Water 356	99
Histidine + Water 356	100
Tryptophan + Water 356	98
Water 456	100
Alanine + Water 456	100
Histidine + Water 456	96
Tryptophan + Water 456	85
Water 556	100
Alanine + Water 556	100
Histidine + Water 556	100
Tryptophan + Water 556	99

2.2.3 Excess polarizability calculations

For each system, we calculated the total box polarizability for 100 configurations, spaced 10 ps apart. To compute the polarizability tensor for each frame, we used CP2K[9] with Goedecker, Teter and Hutter (GTH) pseudopotentials[10] and the revPBE exchange-correlation functional[11,12] with D3 dispersion corrections[13] added.

The maximum polarizability of each frame, α_{max}, was obtained by diagonalizing the polarizability tensor and using the maximum eigenvalue. To compute the excess polarizability, α_{ex}, for each frame, we computed $\alpha_{ex} = \alpha_{max} - \langle\alpha_{iso}\rangle$, where $\langle\alpha_{iso}\rangle$ is the ensemble average of the isotropic polarizability over the water box trajectory of the corresponding number of water molecules and the isotropic polarizability is defined as the average of the eigenvalues obtained from diagonalizing the polarizability tensor[14]. The average α_{ex} values for each system are as follows:

System	Average α_{ex} (Å^3)
Alanine + Water 256	7.45
Histidine + Water 256	17.01
Tryptophan + Water 256	28.00
Alanine + Water 356	9.84
Histidine + Water 356	19.40
Tryptophan + Water 356	27.81
Alanine + Water 456	10.98
Histidine + Water 456	19.74
Tryptophan + Water 456	31.17
Alanine + Water 556	11.19
Histidine + Water 556	20.83
Tryptophan + Water 556	30.24

The values of α_{ex} , as shown in Figure S5, are largely independent of box size.

Even as the average values of α_{ex} calculated from the isotropic polarizability are shown above, we also investigated the maximum component of the polarizability tensor, and how α_{ex} calculated from this value changes over time. As shown in Figure S6, the

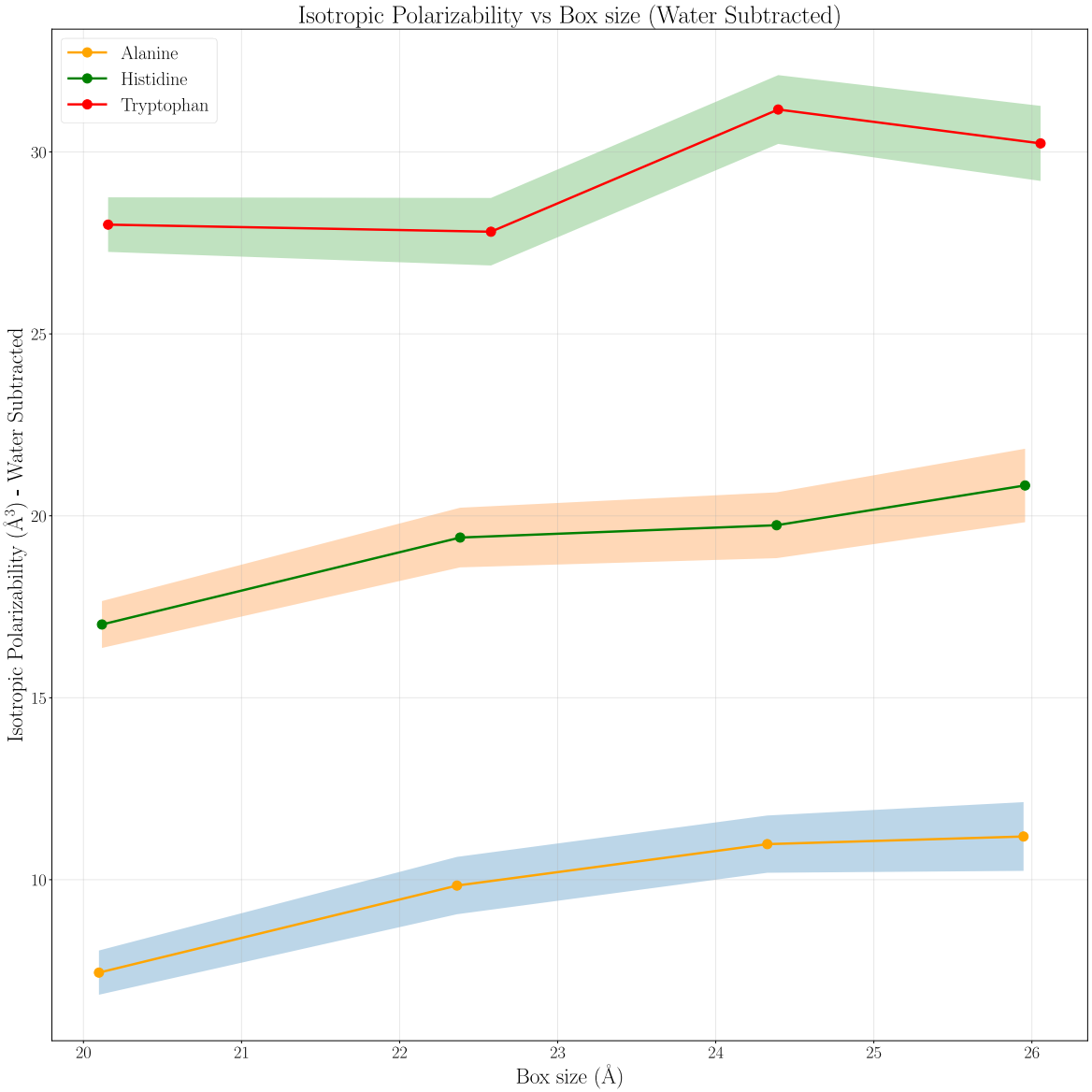

Figure S4 A plot of the water subtracted average isotropic polarizability of alanine, histidine, and tryptophan versus the box size. The shaded regions represent +/- 1 standard deviation.

maximum values of the polarizability tensor can be quite a bit larger than the isotropic value with fluctuations to even larger values.

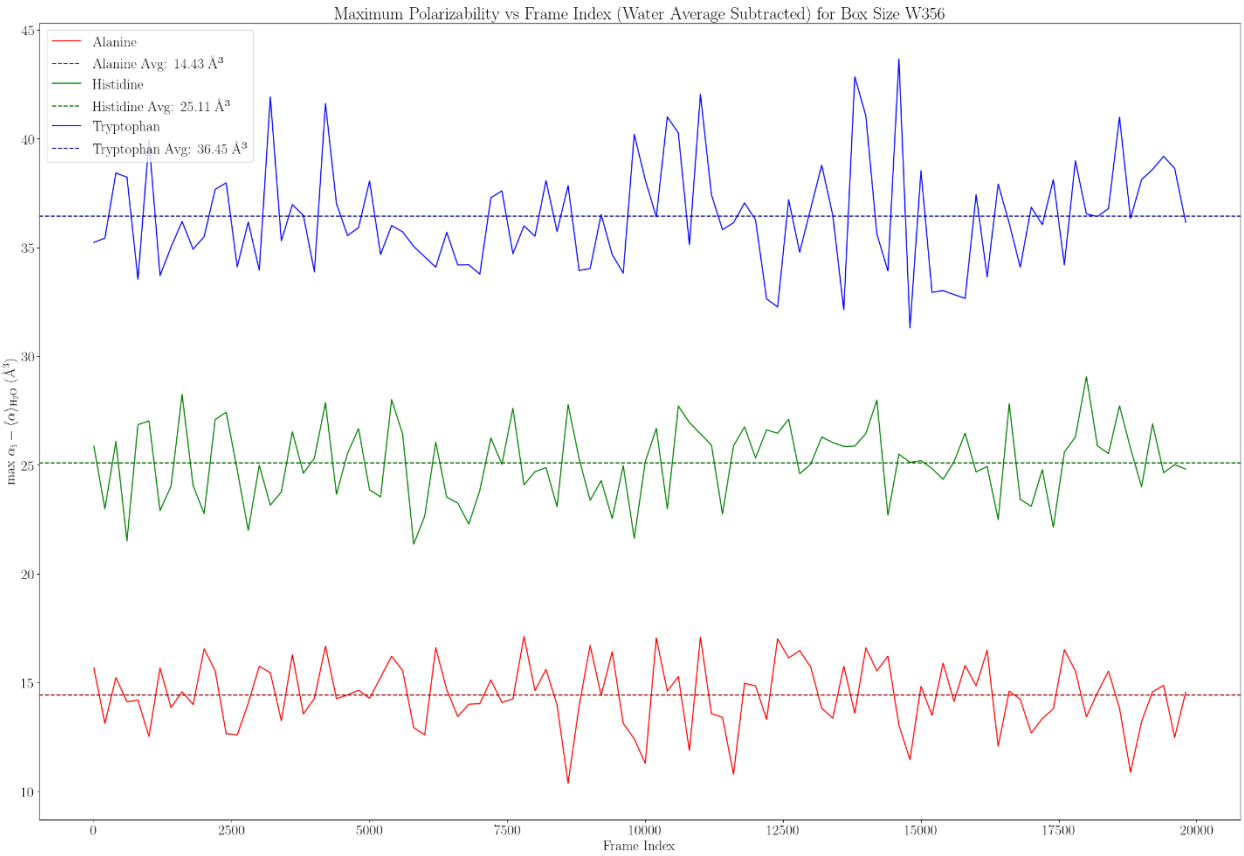

Figure S7 A plot depicting the fluctuations in α_{ex} as a function of frame index for the *maximum* value of the polarizability tensor. Three amino acids are depicted here: alanine, histidine, and tryptophan.

3 Data Analysis

3.1 Resonance Shift of Less than 1 Part 10^5

In the main manuscript, a preliminary guess of the resonance shift due to a single amino acid is calculated as less than 1 part in 10^5. The resonance shift that a molecule exerts on the optical mode of the FFPC can be calculated using the method explained in Saavedra et al[2] in the Supplemental Section 10. For simplicity, the same FFPC parameters were used and an excess polarizability of 25 $Å^3$ for tryptophan as calculated by Zossimova et al was used[14]. Using these two sets of information, the resonance shift that tryptophan is expected to exhibit to the FFPC was calculated to be 1.094 kHz. If we assume that a typical linewidth of our FFPC is 200 MHz then the resonance shift exhibited by an amino acid to the FFPC is less than 1 part in 10^5.

3.2 Signal to Noise Calculation

To calculate the signal-to-noise ratio, the method outlined in Needham et al was used[1]. This method utilized a moving average with different bin sizes to smooth the data, using the following equation:

$$F_{smoothed,i} = \frac{\sum_{j=i}^{i+(n-1)} F_{raw,j}}{n} \quad (1)$$

where n is the bin size and F_i is the value of the function at index i. The bin sizes used ranged from 10 to 300. After smoothing the data, the standard deviation of the longest segment of uninterrupted background was taken and the average of the 10 tallest peak amplitudes from one file were taken to calculate the signal to noise ratio, although the peak amplitude exhibited very little variation due to the saturating behavior of the system. These results can be seen for alanine in the figure below. As shown in the below figure, smoothing has only a marginal effect on signal-to-noise ratio until large bin sizes are used.

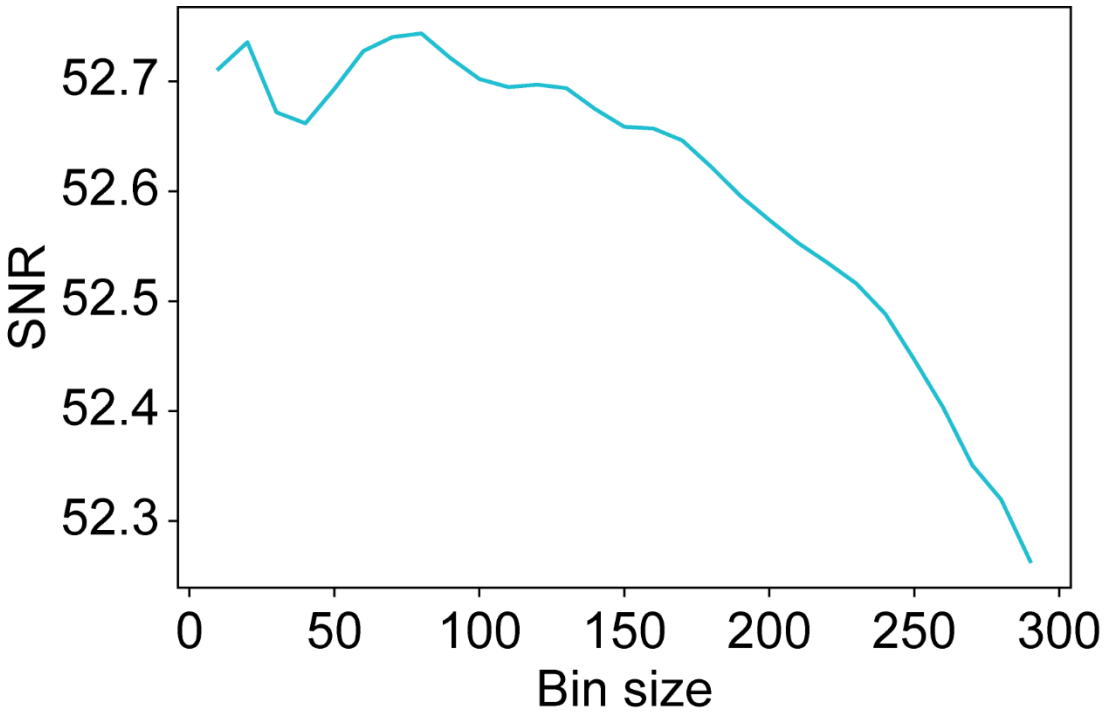

Figure S8 A graph showing signal-to-noise ratios when using different bin sizes for the moving average. This data corresponds to the alanine data from Figure 2.

3.3 Pulse Counting

Below are different plots underlying the data in main manuscript Figure 4a, Fraction Pulses Detected vs Frequency Shift. In all cases, the system response (blue) is shown to a single square input pulse (green). In some cases, it is clear if the pulse has triggered a system response (a) or failed to trigger a system response (b). But, there are cases where spurious signal was observed (c) and cases where there was system instability before the input pulse (d). In both of these cases (c-d), the pulse was not "counted" as having triggered a response.

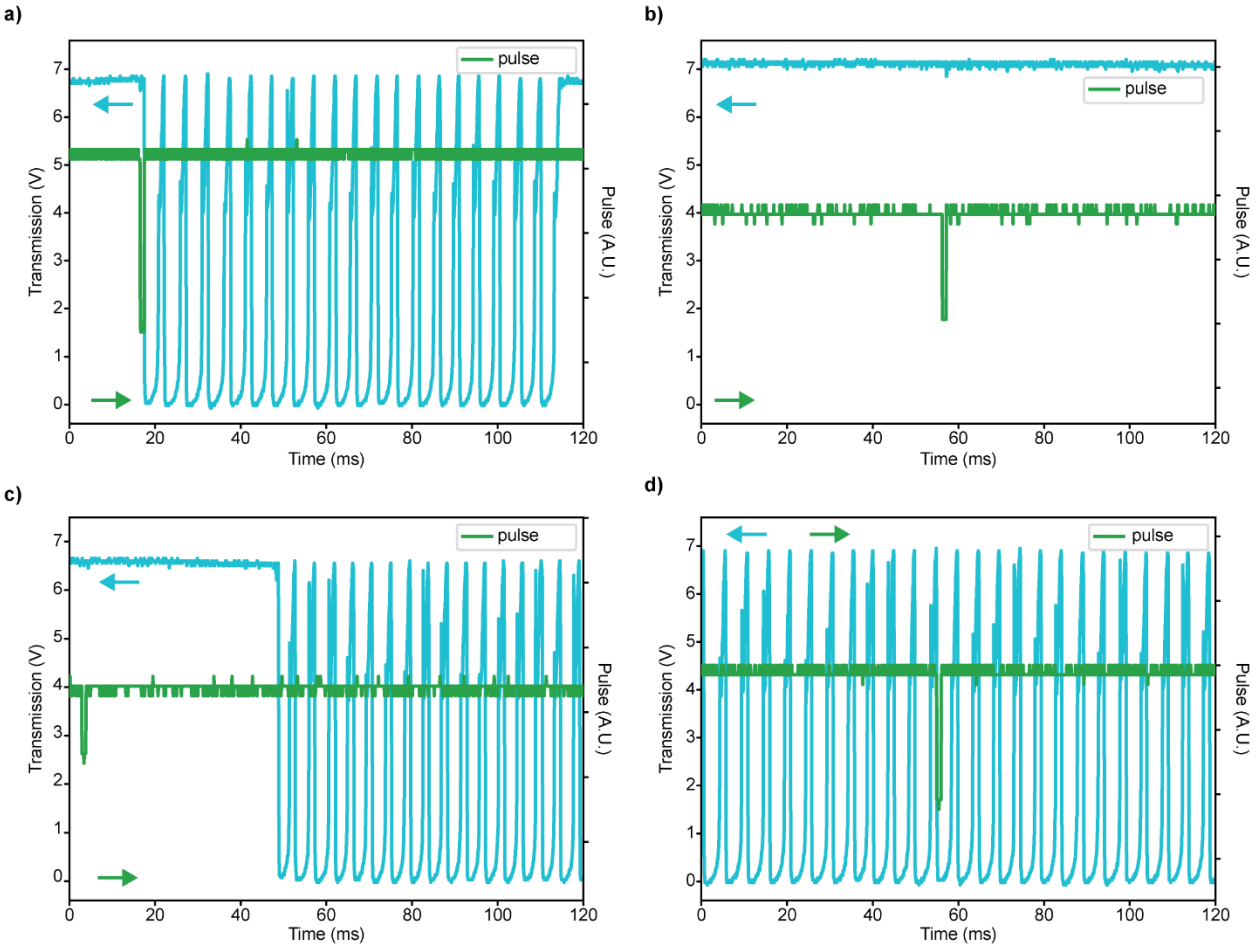

Figure S9. a) Transmission over time showing an input pulse that generated a cavity response. b) Transmission over time showing an input pulse that did not generate a cavity response. c) Transmission over time showing an input pulse and a subsequent cavity response not correlated with an input pulse. d) Transmission over time showing an input pulse that happened within the duration of a cavity response. Small green/blue arrows indicate correlation between trace and y-axis.

3.4 Calculating Finesse and Disagreement with Past Calculations

Finesse was calculated by applying sidebands of a known frequency using a phase modulator (Jenoptik, PM650) driven by a voltage-controlled oscillator (Windfreak, SynthHD PRO) to the resonant mode. This then allowed for a Lorentzian to be fit to the resonance and a linewidth in frequency units to be extracted. The quality factor (Q) could then be calculated:

$$Q = \frac{\nu}{\Delta\nu} \tag{2}$$

where ν is the frequency of the resonant mode and $\Delta\nu$ is the fullwidth half max (FWHM) of the resonant mode. Using the Q factor, finesse can be calculated as follows:

$$F = \frac{Q\lambda}{2nL} \tag{3}$$

where λ is the wavelength of the resonant mode, n is the refractive index of the optical mode, and L is the pathlength of the optical mode. To calculate finesse, Q, λ, and n are now known and L was obtained through an image of the mirror separation. Often, n is dropped from the equation as most FFPC experiments are performed in vacuum or air where the refractive index is essentially one. However, when we are performing our experiments in water this term cannot be ignored. In our previous publication[1], when reporting finesse values in water, they were not divided by the refractive index of water, meaning to compare them to the finesse values reported here, they would need to be divided by 1.33. Importantly, any finesse values reported in air are still comparable and accurate.

3.5 Note on Equation 1 in Main Manuscript

Equation 1 in the main manuscript is only valid when m>>1. A more thorough explanation description of the resonance condition can be found in Kogelnik et al[15].

4 Additional Experimental Details

4.1 Water Controls

For each experiment water controls were collected both before and after data collection with amino acids. Below are examples of water controls. Generally, water controls are blank but there are times where a few spurious traces are detected as represented in Figure S8. Importantly, the statistical analysis in Figure 4b-d include these spurious events.

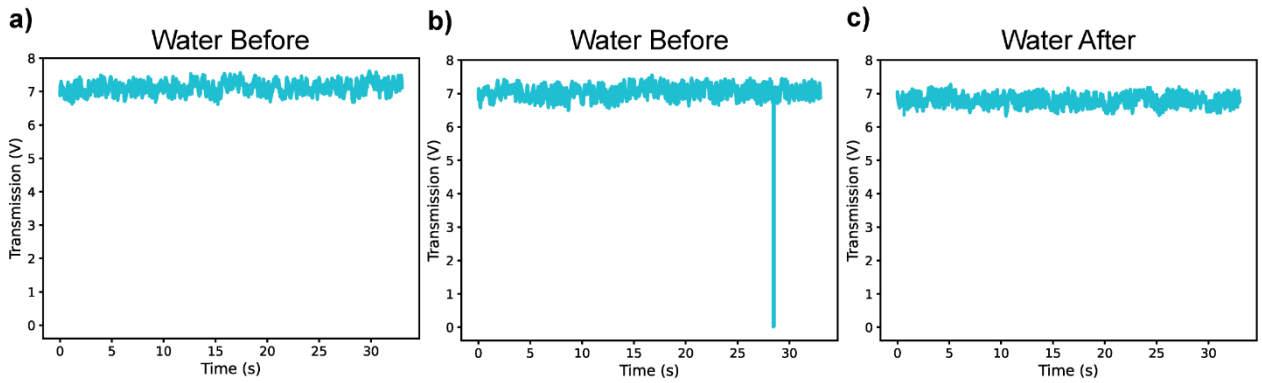

Figure S10 a) A blank water transmission trace taken before histidine data shown in main Fig 2. b) A water transmission trace also taken before histidine data shown in main Fig 2 with an example of a spurious event. c) A blank water trace taken after histidine data shown in main Fig 2.

4.2 Alanine and Alanine Dimer Comparison

Distinguishing between alanine and an alanine dimer offers additional proof of single molecule detection. The FFPC system was tuned to a region where detection of alanine was shown to not be possible (compare Figure S9a with Figure 4a, yellow). In Figure S9, using the differentiation method described in the main text, differentiation between alanine and alanine dimer is achieved. With both the successful differentiation between species and the sensitivity of the FFPC set to a region where alanine should not be detected, this comparison provides evidence that dimers or larger aggregate impurities are not what is being detected in Figure 4.

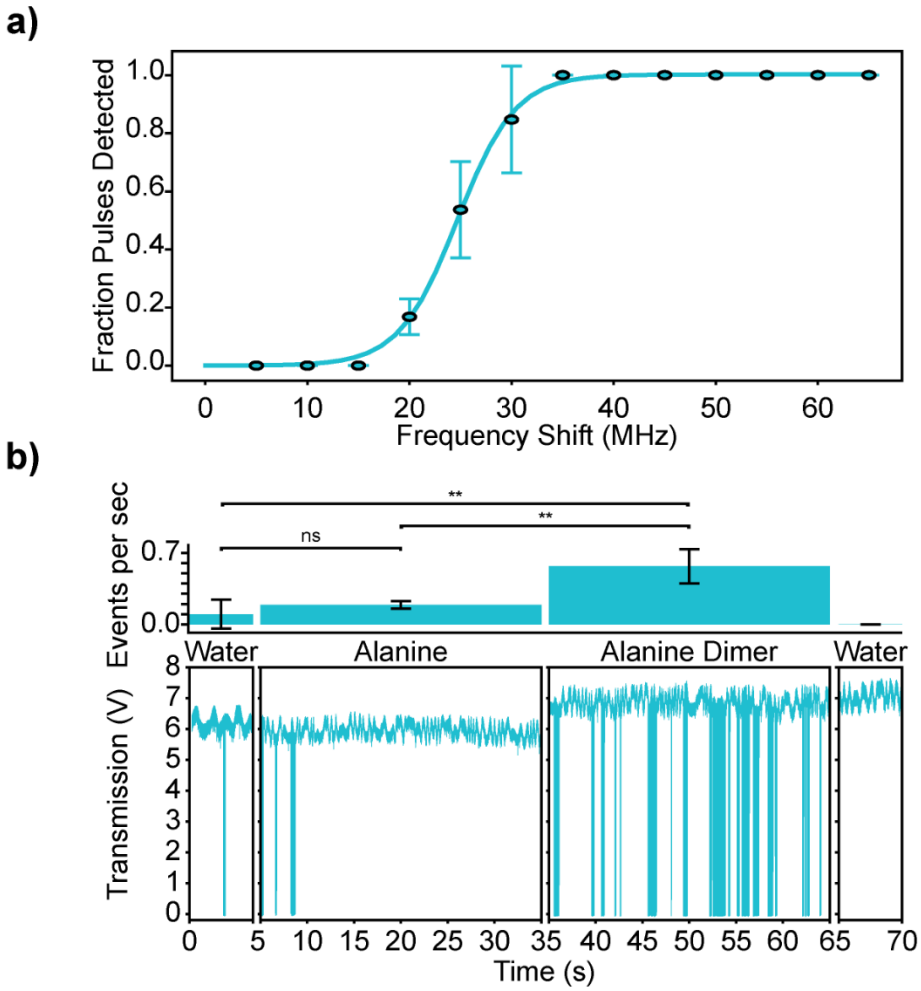

Figure S11 A bar graph depicting a comparison experiment between alanine and an alanine dimer. The difference between the number of detected events between alanine and its dimer were found to be statistically significant. Little to no events were observed in the water controls before and after the experiment. *Asterisks indicate statistical significance:*

ns $p > 0.05$, * $p \leq 0.05$, ** $p \leq 0.01$, *** $p \leq 0.001$, **** $p \leq 0.0001$

4.3 Linearity with Increasing Concentration

To validate that signals in the FFPC were due to single molecules, the response of the system with respect to concentration was measured. To do this experiments were performed by beginning with water controls. After taking water controls, the amino acid was added to the FFPC at 5 pM and traces were recorded. The sample was then exchanged for 10 pM by pipetting the 10 pM solution on and off the FFPC a few times. After, traces were recorded at 10 pM. The same process was repeated for 15 and 20 pM samples. Like all experiments, water controls were taken at the end following a cleaning procedure involving pipetting water off and on the FFPC.

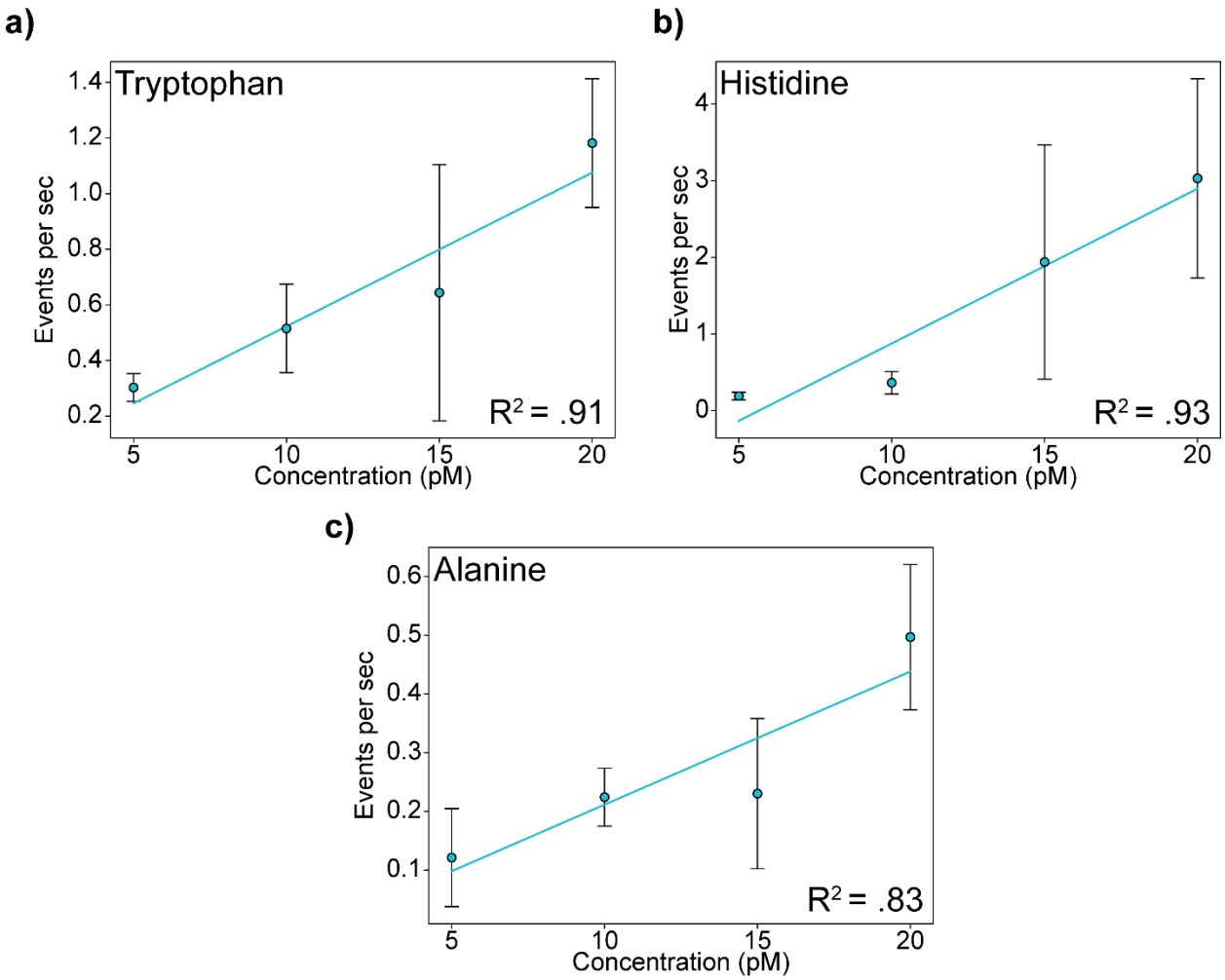

Figure S12 Graphs depicting the linearity of the rate of events versus concentration. a) The response from tryptophan. b) The response from histidine. c) The response from alanine.

4.4 Sensitivity Plots Before and After Amino Acid Data Collection

To ensure that the FFPC did not change drastically during the experiment, sensitivity pulse plots were collected before and after collecting amino acid data. Some drift in system sensitivity here is expected due to the cleaning of the cavity which causes some slight mechanical perturbations resulting in a minor change in sensitivity.

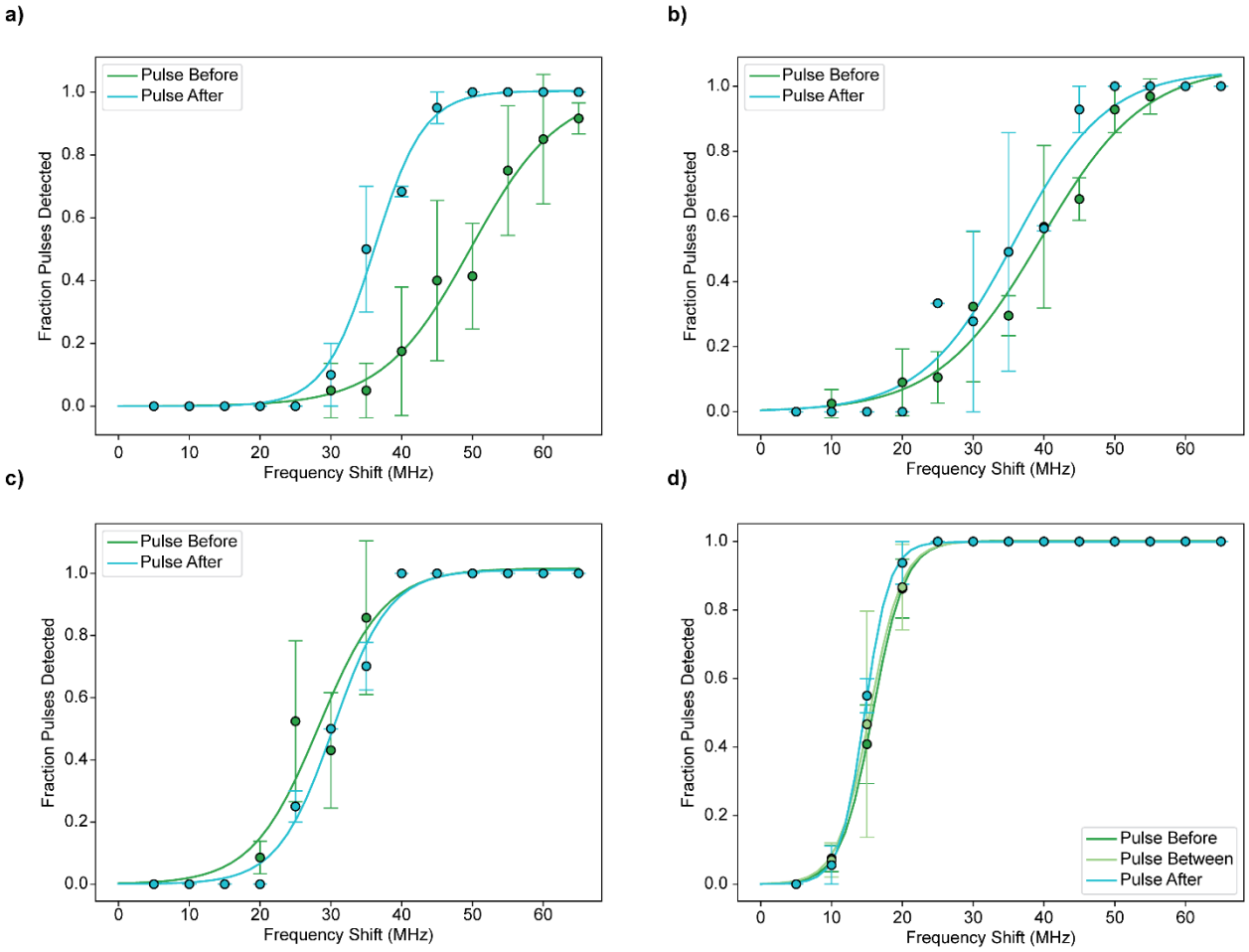

Figure S13 Plots showing the calibrations before and after for the comparisons in Figure 4. a) The comparison between tryptophan and Myc-tag b) The comparison between histidine and tryptophan c) The comparison between alanine and histidine d) The comparison between glycine and alanine. Here, a series of test pulses were included in between examining the two amino acids as well.

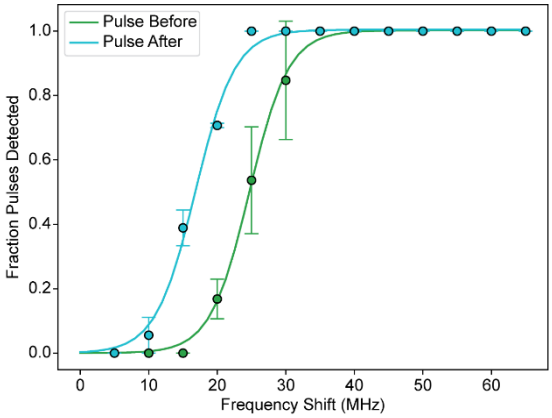

Figure S15 A plot showing the calibrations before and after for the comparison between alanine and its dimer.

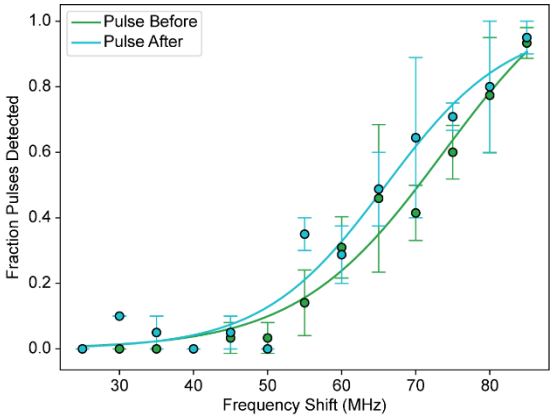

Figure S14 A plot showing the calibrations before and after for the comparison between threonine and threonine with a PTM.

4.5 Locking Bandwidth Experiment and Calculations

The locking bandwidth (LBW) of the experiment refers to the frequency at which the PI can respond to and suppress different frequency perturbations. Measuring the LBW is important to understanding one of the lower boundary of the molecular detection window.

The locking bandwidth (LBW) was measured using the Frequency Response Analyzer function of the Liquid Instruments Moku:Go following the protocol in Saavedra et al[3]. The PDH error signal was fed into the input of the frequency response analyzer. The PDH error signal was then summed with the varying sinusoidal perturbation produced by the analyzer and then fed into the PI lockbox. The frequency response was measured from 10 Hz to 10kHz with 2 millisecond averaging duration and 10 cycles per frequency response measured. The loop gain ($CSM(v)$) was calculated using the equation shown below where A is equal to the signal voltage gain (c) times the phase factor.

$$CSM(v) = \frac{-A}{(A+1)}, A = ce^{i\phi} \quad (4)$$

The LBW is the unity gain frequency or where $|CSM(v)| = 1$, as shown by the dashed lines in Figure S14. At the locking settings used in Figure S14, which were comparable to those used for the experiment shown in the Figure 5, the LBW is 190 Hz.

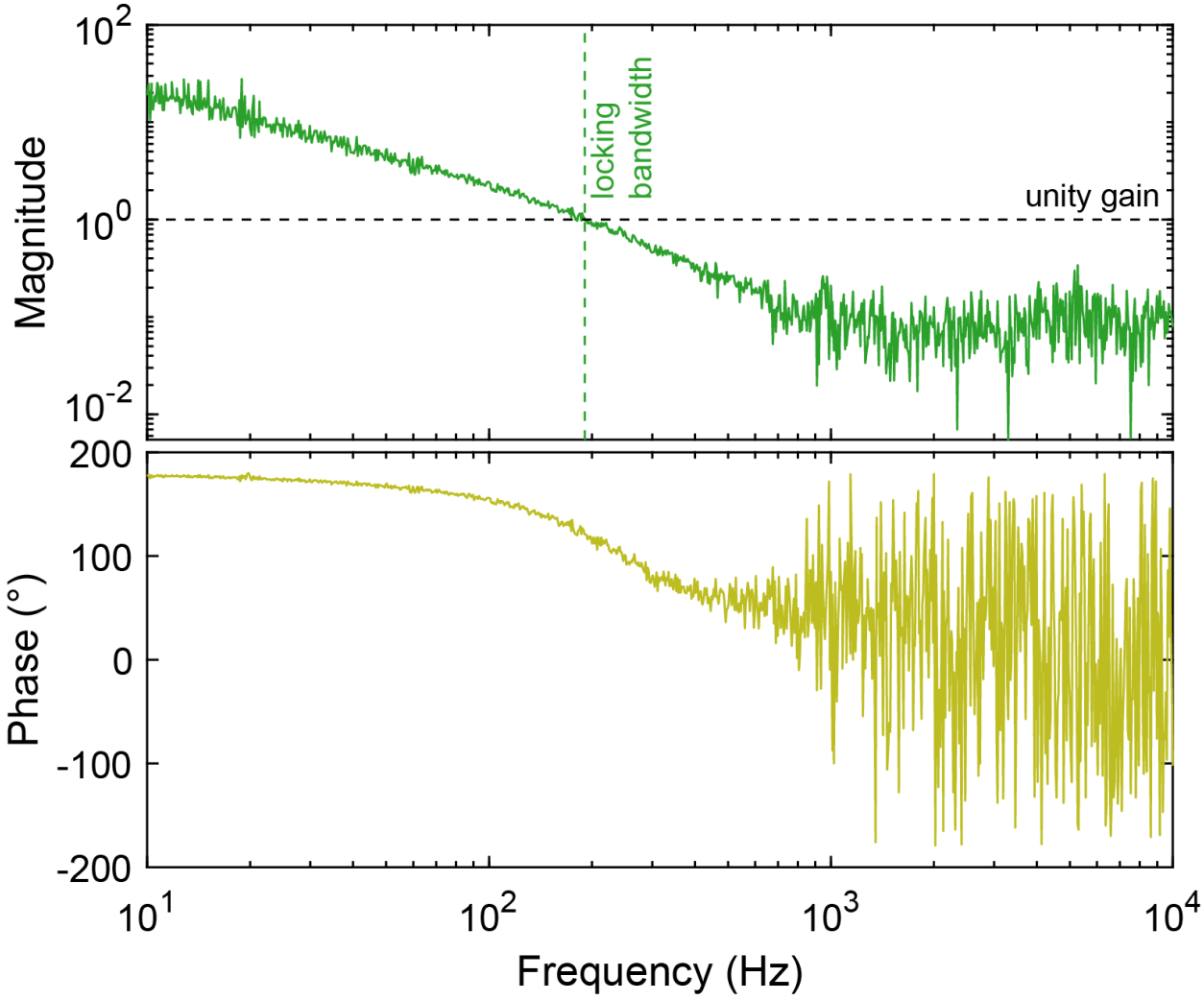

Figure S16 Plots depicting the magnitude and phase as measured by the frequency response analyzer function on the MokuGo. The zero point crossing on the magnitude plot shows the locking bandwidth to be 190 Hz.

5 Supplementary References

1 Needham, L.-M. *et al.* Label-free detection and profiling of individual solution-phase molecules. *Nature* **629**, 1062-1068 (2024). https://doi.org/10.1038/s41586-024-07370-8

2 Saavedra Salazar, C. A. *et al.* The Origin of Single-Molecule Sensitivity in Label-Free Solution-Phase Optical Microcavity Detection. *ACS Nano* **19**, 6342-6356 (2025). https://doi.org/10.1021/acsnano.4c16276

3 Saavedra, C., Pandey, D., Alt, W., Pfeifer, H. & Meschede, D. Tunable fiber Fabry-Perot cavities with high passive stability. *Opt. Express* **29**, 974-982 (2021). https://doi.org/10.1364/OE.412273

4 Germann, M. W., Turner, T. & Allison, S. A. Translational Diffusion Constants of the Amino Acids: Measurement by NMR and Their Use in Modeling the Transport of Peptides. *The Journal of Physical Chemistry A* **111**, 1452-1455 (2007). https://doi.org/10.1021/jp068217o

5 Meng, E. C. *et al.* UCSF ChimeraX: Tools for structure building and analysis. *Protein Science* **32**, e4792 (2023). https://doi.org/https://doi.org/10.1002/pro.4792

6 Eastman, P. *et al.* OpenMM 8: Molecular Dynamics Simulation with Machine Learning Potentials. *The Journal of Physical Chemistry B* **128**, 109-116 (2024). https://doi.org/10.1021/acs.jpcb.3c06662

7 Huang, J. & MacKerell Jr, A. D. CHARMM36 all-atom additive protein force field: Validation based on comparison to NMR data. *Journal of Computational Chemistry* **34**, 2135-2145 (2013). https://doi.org/https://doi.org/10.1002/jcc.23354

8 Jorgensen, W. L., Chandrasekhar, J., Madura, J. D., Impey, R. W. & Klein, M. L. Comparison of simple potential functions for simulating liquid water. *The Journal of Chemical Physics* **79**, 926-935 (1983). https://doi.org/10.1063/1.445869

9 Hutter, J., Iannuzzi, M., Schiffmann, F. & VandeVondele, J. cp2k: atomistic simulations of condensed matter systems. *WIREs Computational Molecular Science* **4**, 15-25 (2014). https://doi.org/https://doi.org/10.1002/wcms.1159

10 Goedecker, S., Teter, M. & Hutter, J. Separable dual-space Gaussian pseudopotentials. *Physical Review B* **54**, 1703-1710 (1996). https://doi.org/10.1103/PhysRevB.54.1703

11 Perdew, J. P., Burke, K. & Ernzerhof, M. Generalized Gradient Approximation Made Simple. *Physical Review Letters* **77**, 3865-3868 (1996). https://doi.org/10.1103/PhysRevLett.77.3865

12 Zhang, Y. & Yang, W. Comment on ``Generalized Gradient Approximation Made Simple''. *Physical Review Letters* **80**, 890-890 (1998). https://doi.org/10.1103/PhysRevLett.80.890

13 Grimme, S., Antony, J., Ehrlich, S. & Krieg, H. A consistent and accurate ab initio parametrization of density functional dispersion correction (DFT-D) for the 94 elements H-Pu. *The Journal of Chemical Physics* **132** (2010). https://doi.org/10.1063/1.3382344

14 Zossimova, E., Fiedler, J., Vollmer, F. & Walter, M. Hybrid quantum-classical polarizability model for single molecule biosensing. *Nanoscale* **16**, 5820-5828 (2024). https://doi.org/10.1039/D3NR05396B